IET Microwaves, Antennas & Propagation

Research Article

IET Journals
The Institution of Engineering and Technology

Co-located and distributed antenna systems: deployment options for massive multiple-input–multiple-output

ISSN 1751-8725
Received on 24th October 2014
Revised on 23rd May 2015
Accepted on 1st June 2015
doi: 10.1049/iet-map.2014.0714
www.ietdl.org

Khawla A. Alnajjar[1,2], Peter J. Smith[2], Graeme K. Woodward[1] ✉

[1]*Wireless Research Centre, University of Canterbury, Private Bag 4800, Christchurch 8140, New Zealand*
[2]*Department of Electrical and Computer Engineering, University of Canterbury, Private Bag 4800, Christchurch 8140, New Zealand*
✉ *E-mail: graeme.woodward@canterbury.ac.nz*

Abstract: To evaluate the benefits of distributed arrays in massive multiple-input–multiple-output systems, the authors investigate the interaction between linear receivers (maximum ratio combining and zero forcing) and three deployments scenarios: (i) a massive co-located array at the cell centre; (ii) a massive array clustered at *B* discrete locations; and (iii) a massive distributed array with a uniform distribution of individual antennas. The authors also study the effect of propagation parameters, system size, correlation and channel estimation error. The authors demonstrate by analysis and simulation that in the absence of any system imperfections, a massive distributed array is preferable. An intermediate deployment such as a massive array clustered at a few discrete locations, can be more practical to implement and more robust to imperfect channel state information. The authors show an example with a 128 antenna deployment where four locations achieves one third of the gains due to a fully distributed array.

1 Introduction

There is growing interest in massive multiple-input–multiple-output (MIMO) techniques [1, 2] for 5th generation wireless systems (5G). This is due to their ability to increase degrees of freedom, reduce transmit power [3], average out small-scale fading, and create quasi-orthogonal user equipments (UEs) [3]. One of the remaining challenges for massive MIMO is the design of an effective antenna deployment strategy. A massive, centralised array is easier to construct and requires less backhaul. In contrast, a fully distributed array is more complex and has higher latency and backhaul requirements, but may provide superior performance.

Most work on massive MIMO assumes co-located arrays but the distributed option has potential for increased throughput and shadow fading diversity [4–7]. The advantage of distributed arrays has been investigated in traditional MIMO systems (<10 antennas) and also for remote radio heads/units and cloud Radio Access Network [7–10]. In this paper, we consider three massive MIMO deployment options: a co-located base station (BS) array (COL); *B* collaborative base stations with multiple antennas (*B*BS); and distributed arrays with geographically separated single antenna base stations (DIST). In *B*BS and DIST, the multiple BSs collaborate perfectly to perform joint detection at some central processor. We assume a standard hexagonal cellular topology with two tiers of interference: a desired cell at the centre and interference cells located in two surrounding tiers. One of the advantages of large arrays is their ability to orthogonalise the channel vectors of different UEs at the co-located BS [3]. Here, the focus is on a different massive MIMO property, a type of averaging over the link gains, which enables us to demonstrate the gains of distributed over co-located deployment. In [4], a downlink finite system analysis was developed using randomly located BSs and in [6, 7], a downlink asymptotic analysis is derived for sum-rate and rate performance, respectively. In [5], an uplink distributed system analysis for signal-to-interference-and-noise-ratio (SINR) is derived from the asymptotic analysis in [1]. The work in [5] is the closest to this paper but it focuses on spatial correlation effects and BS grouping. We take a different approach, simplifying the analysis further while maintaining accuracy and deriving insights into maximum ratio combining (MRC) and zero forcing (ZF) receivers, deployment options and propagation conditions. In this paper, uplink performance is considered using linear receivers with fixed BS locations. MRC and ZF are used because they are particularly relevant in massive MIMO due to their relatively low complexity [2].

The main contributions of this paper are:

- remarkably simple and accurate analytic approximations to the SINR at the output of massive MIMO linear receivers;
- use of the analytical results to explain the effects of path loss, shadowing, channel estimation error, channel correlation and system size;
- analysis and simulation to evaluate the performance of an intermediate deployment, where the massive array is spread over *B* locations (*B*BS);
- analysis and simulations to evaluate the deployment scenarios under differing levels of interference (different frequency re-use factors) and with different geographic spreads of the antenna arrays within the cell.

In the following, the system model and deployment scenarios are given in Sections 2 and 3. Sections 4–6 provide analysis, results and conclusions.

2 System model for uplink cellular layout

A cellular structure is considered with 19 hexagonal cells, where the centre cell contains the desired UEs and there are two surrounding interference tiers (top left-hand side, Fig. 1). In each cell, a BS with N_r receive antennas serves N_t single antenna UEs and $N_f \leq 18N_t$ is the number of interferers in the first and second interference tiers that share resources with the centre cell, such as frequency and time. For this uplink model, the received signal is given by

$$\begin{aligned} \boldsymbol{y} &= \boldsymbol{H}\boldsymbol{x} + \boldsymbol{F}\boldsymbol{x}_I + \boldsymbol{n} \\ &= \underbrace{\boldsymbol{h}_1 x_1}_{\text{desired signal}} + \underbrace{\sum_{m=2}^{N_t} \boldsymbol{h}_m x_m}_{\text{intra-cell interference}} + \underbrace{\sum_{m=1}^{N_f} \boldsymbol{f}_m x_{I_m}}_{\text{inter-cell interference}} + \underbrace{\boldsymbol{n}}_{\text{noise}}, \end{aligned} \quad (1)$$

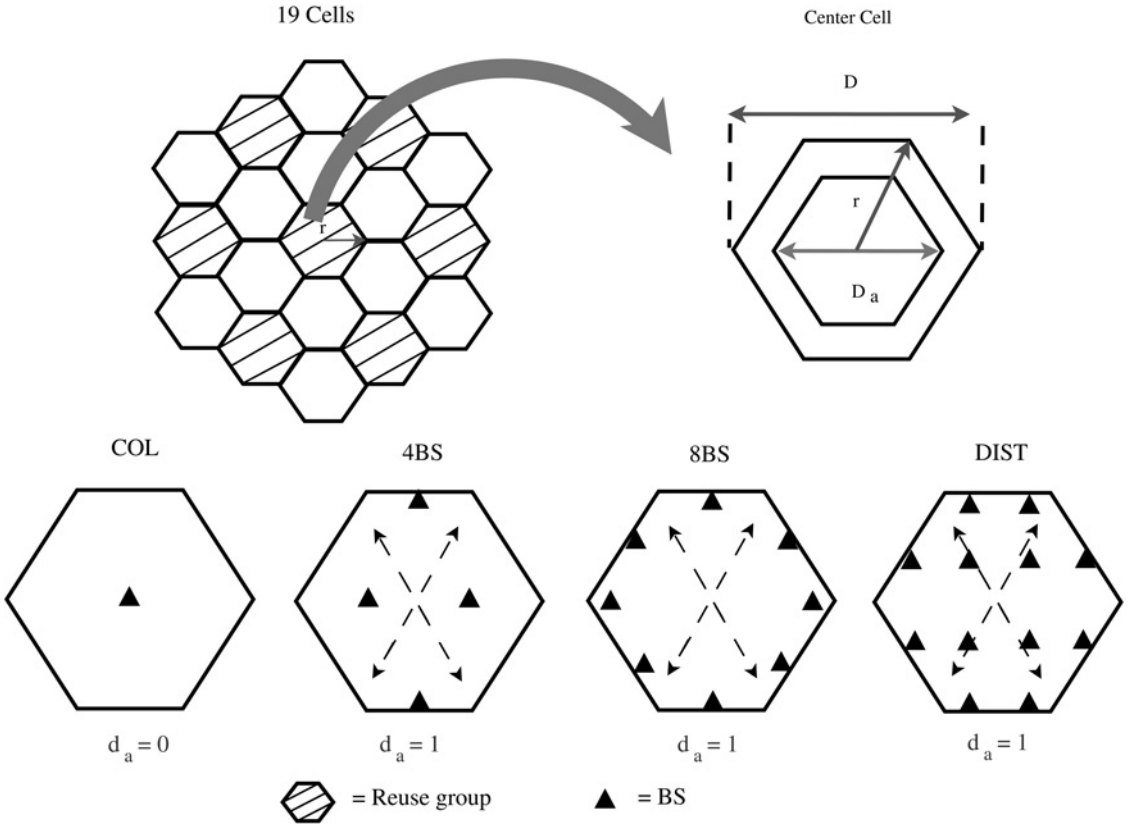

Fig. 1 *Example of deployment scenarios*

where $\boldsymbol{H} = \left[\boldsymbol{h}_1 \cdots \boldsymbol{h}_{N_t}\right]$ is the $N_r \times N_t$ channel matrix of the UEs located in the centre cell, $\boldsymbol{F} = \left[\boldsymbol{f}_1 \cdots \boldsymbol{f}_{N_f}\right]$ is the $N_r \times N_f$ channel matrix of UEs located in the other cells and Rayleigh fading is assumed for all channels. The remaining terms in (1) are defined as follows. The $N_t \times 1$ vector of transmitted symbols from centre cell UEs is $\boldsymbol{x} = \left[x_1, x_2, \ldots x_{N_t}\right]^T$ while the $N_f \times 1$ vector of transmitted symbols from other cell UEs is $\boldsymbol{x}_I = \left[x_{I_1}, x_{I_2}, \ldots x_{I_{N_f}}\right]^T$. The received signals are corrupted by the $N_r \times 1$ noise vector, $\boldsymbol{n} = [n_1 \ldots n_{N_r}]^T$, with independent and identically distributed (i.i.d.) complex Gaussian elements, $n_i \sim \mathcal{CN}(0, \sigma^2)$. Without loss of generality the transmit symbols satisfy $E\left[\left|x_j\right|^2\right] = E\left[\left|x_{I_j}\right|^2\right] = 1$ and so the signal to noise ratio (transmit SNR) is given by $\rho = E\left[\left|x_j\right|^2\right] / \sigma^2 = 1/\sigma^2$. The channel coefficient, h_{ij}, from UE j inside the centre cell to receive antenna i has the link gain $E\left[\left|h_{ij}\right|^2\right] = P_{ij}$, whereas the channel coefficient, f_{ij}, from UE j outside the centre cell to receive antenna i has the link gain $E\left[\left|f_{ij}\right|^2\right] = Q_{ij}$.

Obtaining accurate channel state information (CSI) is one of the challenges in massive MIMO due to pilot contamination [2] and in distributed scenarios there are also likely to be latency issues [11]. Thus, the simple equivalent channel estimation model [12] is used, where the true channel, $\boldsymbol{H}$, is given by $\boldsymbol{H} = r_0\widehat{\boldsymbol{H}} + \sqrt{1 - r_0^2}\boldsymbol{E}$, where r_0 is the correlation coefficient between $\boldsymbol{H}$ and the estimated channel $\widehat{\boldsymbol{H}}$, and $\boldsymbol{E} = \left[\boldsymbol{e}_1 \cdots \boldsymbol{e}_{N_t}\right]$ has the same statistics as $\boldsymbol{H}$.

In this paper, we consider linear detectors where the output of the linear combiner, $\boldsymbol{W}$, has the form, $\boldsymbol{W}^H\boldsymbol{y}$, where $\boldsymbol{W}^H$ represents the complex conjugate transpose of $\boldsymbol{W}$. For any such combiner, the output SINR (the mean signal power divided by the mean interference plus noise power) for the mth UE is calculated using a simple variation of the SINR in [13, (9)] as

$$\mathrm{SINR}_m = \frac{E\left[\left|r_0 \boldsymbol{w}_m^H \widehat{\boldsymbol{h}}_m x_m\right|^2\right]}{E\left[\left|\boldsymbol{w}_m^H\left(r_0 \sum_{j \neq m} \widehat{\boldsymbol{h}}_j x_j + \sqrt{1 - r_0^2}\boldsymbol{E}\boldsymbol{x} + \boldsymbol{F}\boldsymbol{x}_I + \boldsymbol{n}\right)\right|^2\right]}, \tag{2}$$

where $\boldsymbol{w}_m$ is the mth column of $\boldsymbol{W}$. Note that the expectation in the numerator and denominator of (2) is with respect to signal and noise. The combiners considered are ZF, where $\boldsymbol{W} = \widehat{\boldsymbol{H}}(\widehat{\boldsymbol{H}}^H\widehat{\boldsymbol{H}})^{-1}$ [14, page 48] and MRC where $\boldsymbol{W} = \widehat{\boldsymbol{H}}$ [15, page 331]. For small systems, typically using 2–8 antennas, MRC is never normally preferred over ZF as it has no capability to reduce interference. However, for massive MIMO the simplicity of MRC is desirable and in certain situations MRC performance approaches that of minimum-mean-squared-error detection [14, page 48] as the system size increases [2]. The precise nature of channels and receivers depends on the BS deployment which is discussed next.

3 Deployment scenarios for the massive array

Massive MIMO can result from a large number of antennas deployed at one location or from an array of distributed antennas linked together to form a massive network MIMO system. The following scenarios are considered for simplicity and are also shown schematically in Fig. 1.

- One massive co-located array (COL).
- B collaborative base stations with multiple antennas at each BS (BBS).
- One massive array with geographically distributed single antenna BSs (DIST).

In these cellular layouts the positions of UEs and BSs is as follows. The UEs are located uniformly and randomly in all cells which have a common radius of r (diameter $D = 2r$). The BSs are located in the inner indented hexagon of the centre cell as in Fig. 1 to study the effects of distributing antennas over varying proportions of the cell. Hence, the BSs are located inside a hexagon of diameter $D_a = d_a D$ where $0 \le d_a \le 1$ is a scaling factor. The special case of $d_a = 0$ corresponds to COL and, in DIST, $d_a = 1$ corresponds to spreading the array over the entire cell. Note that Fig. 1 shows only 12 antennas in DIST for clarity whereas we consider 128 antennas in the array because a regular grid of 128 points fits almost symmetrically in a hexagon giving an even spread of antennas over the cell in DIST. Thus, the specific deployments are: COL: 128 co-located antennas at the centre of the coverage area; 4BS: 4 BS locations each with 32 antennas at each of the positions $\left(0, -\sqrt{3}/4\right)$, $(-0.25, 0)$, $\left(0, -\sqrt{3}/4\right)$ and $(0.25, 0)$ for $d_a = 1$ and $D = 1$; 8BS: 8 BS locations located in a circle each with 16 antennas; and DIST: 128 single antenna BSs. Note that optimal placement of the BSs is beyond the scope of this paper and we select simple examples of possible locations for 4BS and 8BS. The 4BS locations span the cell with $\left(0, \pm\sqrt{3}/4\right)$ lying on the cell edge and the other 2 BSs located at $(\pm 0.25, 0)$ were chosen to be half way to the cell edge to increase the SINR values. Various levels of interference from the two interference tiers in the cell layout of Fig. 1 are considered. The interference scenarios are: no interference (nCells = 1), interference from the 6 cells located in the first interference tier (nCells = 7), interference from the 18 cells located in both interference tiers (nCells = 19), and interference from the 6 shaded cells located in the frequency reuse group of size 3 (nCells = 19, reuse 3).

For all scenarios, we adopt the classical channel model where

$$\boldsymbol{H} = \boldsymbol{R}_{\mathrm{r}}^{1/2}\boldsymbol{G}, \tag{3}$$

$G_{ij} = \sqrt{P_{ij}}U_{ij}$, the $U_{ij} \sim \mathcal{CN}(0, 1)$ are i.i.d. fast fading terms, $\boldsymbol{R}_{\mathrm{r}}^{1/2}$ is the spatial correlation matrix at the receive array and P_{ij} is the link gain defined by [16, page 104]

$$P_{ij} = AL_{ij}d_{ij}^{-\gamma}. \tag{4}$$

The terms in (4) as follows. A is a constant depending on transmit power, antenna height etc. L_{ij} is a lognormal shadow fading variable defined by $L_{ij} = 10^{\mathcal{L}_{ij}/10}$, where $\mathcal{L}_{ij}$ is an i.i.d. complex Gaussian variable with zero mean and constant shadow fading variance σ_{SF}^2 and d_{ij} is link distance. Including the effects of spatial correlation in the shadow fading is critical here because small values of d_a bring the antennas close together and in this situation independent shadowing is unrealistic. The correlation between the shadow fading terms at antennas i and j, is defined by $\bar{R}_{ij} = \mathrm{e}^{-r_{ij}/(br)}$ with r_{ij} being the antenna separation and $b \in [0, 1]$ is the fraction of the cell radius at which decorrelation occurs, that is, at which $\bar{R}_{ij} = e^{-1}$. Note that $\bar{R}_{ij} = E\left[10\log_{10}L_{ik} \times 10\log_{10}L_{jk}\right]$ for any UE, $k = 1, 2, \ldots, N_{\mathrm{t}}$. This is the well-known exponential correlation model [17] and typical values of b in the literature range from 0.1 to 0.5 [18]. For simplicity, we assume a constant A and a constant path loss exponent, γ. The difference between the channel coefficients for the scenarios lies solely in the structure of the link gains. For COL, $P_{ij} = P_j = AL_j d_j^{-\gamma}$, as all N_{r} paths from UE j to the BS have the same power defined by a single shadow fading variable, L_j and a single distance, d_j. In BBS, each UE has B link gains. These powers are defined by $P_{ij} = P_j^{(k)} = AL_j^{(k)}\left(d_j^{(k)}\right)^{-\gamma}$, where $k = \{1\ldots, B\}$, the B lognormals are independent, distances are distinct and k is the index of the BS. Here, k replaces the index i as the powers depend on the BS, not on the individual antenna. For DIST, $P_{ij} = AL_{ij}d_{ij}^{-\gamma}$ where L_{ij} are correlated shadow fades and d_{ij} are the distances from UE j to the 128 BSs. Similarly, f_{ij} has the same structure as h_{ij}, where $f_{ij} = \sqrt{Q_{ij}}\mathcal{V}_{ij}$, Q_{ij} is the link gain and $\mathcal{V}_{ij} \sim \mathcal{CN}(0, 1)$ are i.i.d. fast fading terms.

The channel correlation matrix at the receiver in (3) has the block diagonal form $\boldsymbol{R}_{\mathrm{r}} = \mathrm{diag}(\boldsymbol{R}_b, \ldots, \boldsymbol{R}_b)$, where $\boldsymbol{R}_b$ is the correlation matrix at each of the B arrays. Let $\boldsymbol{R}_b = (R_{ij})$, then the element R_{ij} is modelled by $R_{ij} = \alpha_u^{|i-j|}$, where α_u is the correlation between channels at adjacent antennas, $0 < \alpha_u < 1$ and $i, j = \{1, \ldots, N_{\mathrm{r}}/B\}$. This is the simple exponential correlation model given in [19]. Therefore, $\boldsymbol{R}_b$ can be decomposed as $\boldsymbol{R}_b = \boldsymbol{\Psi}_b^{\mathrm{H}}\boldsymbol{\Lambda}_b\boldsymbol{\Psi}_b$, where $\boldsymbol{\Psi}_b$ is a unitary matrix and $\boldsymbol{\Lambda}_b$ is a diagonal matrix containing the eigenvalues of $\boldsymbol{R}_b$.

4 SINR analysis for ZF and MRC

In this section we analyse the effects of propagation parameters and the BS deployment scenarios described in Section 3 on MRC and ZF performance.

4.1 Exact SINR calculations

For a ZF receiver and UE 1, the general SINR in (2) collapses to [20]

$$\mathrm{SINR}_1^{(\mathrm{ZF})} = \frac{r_0^2}{\left[(\boldsymbol{W}^{\mathrm{H}}\left((1-r_0^2)\boldsymbol{E}\boldsymbol{E}^{\mathrm{H}} + \boldsymbol{F}\boldsymbol{F}^{\mathrm{H}} + \sigma^2\boldsymbol{I}\right)\boldsymbol{W}\right]_{11}}, \tag{5}$$

where $[.]_{11}$ denotes the (1,1)th element of a matrix. For an MRC receiver, the SINR for UE 1 is given by (see (6))

Every term in (5) and (6) is constructed from the cross products $\widehat{\boldsymbol{h}}_i^{\mathrm{H}}\widehat{\boldsymbol{h}}_j$, $\widehat{\boldsymbol{h}}_i^{\mathrm{H}}\boldsymbol{e}_j$ and $\widehat{\boldsymbol{h}}_i^{\mathrm{H}}\boldsymbol{f}_j$. Since all UEs experience the same correlations, $\widehat{\boldsymbol{h}}_j$, $\boldsymbol{e}_j$ and $\boldsymbol{f}_j$ all have the same correlation matrix. Hence, each cross product is of the form $\breve{\boldsymbol{x}}^{\mathrm{H}}\breve{\boldsymbol{y}} = \tilde{\boldsymbol{x}}^{\mathrm{H}}\boldsymbol{R}_{\mathrm{r}}^{1/2}\boldsymbol{R}_{\mathrm{r}}^{1/2}\tilde{\boldsymbol{y}}$ where $\tilde{\boldsymbol{x}}$, $\tilde{\boldsymbol{y}}$ have the same power structure as $\breve{\boldsymbol{x}}$, $\breve{\boldsymbol{y}}$, but are independent. Using the eigenvalue

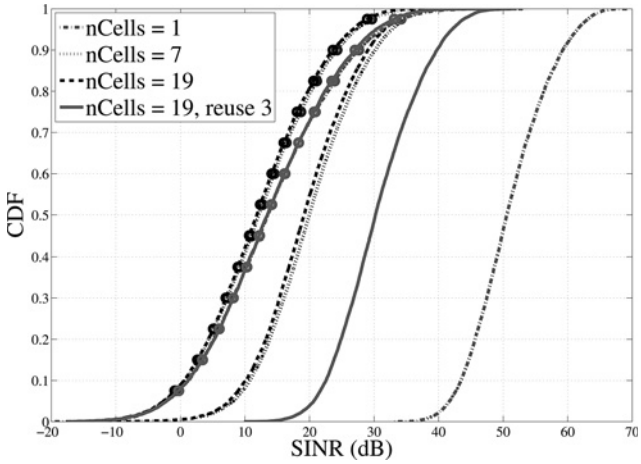

Fig. 2 *SINR CDFs for the DIST scenario with ZF and MRC and differing numbers of interfering cells. Lines alone represent ZF and lines with circles represent MRC. nCells ∈ {1, 7, 19}*

$$\mathrm{SINR}_1^{(\mathrm{MRC})} = \frac{r_0^2\left|\widehat{\boldsymbol{h}}_1^{\mathrm{H}}\widehat{\boldsymbol{h}}_1\right|^2}{r_0^2\sum_{j=2}^{N_t}\widehat{\boldsymbol{h}}_1^{\mathrm{H}}\widehat{\boldsymbol{h}}_j\widehat{\boldsymbol{h}}_j^{\mathrm{H}}\widehat{\boldsymbol{h}}_1 + \left(1-r_0^2\right)\sum_{j=1}^{N_t}\widehat{\boldsymbol{h}}_1^{\mathrm{H}}\boldsymbol{e}_j\boldsymbol{e}_j^{\mathrm{H}}\widehat{\boldsymbol{h}}_1 + \sum_{j=1}^{N_f}\widehat{\boldsymbol{h}}_1^{\mathrm{H}}\boldsymbol{f}_j\boldsymbol{f}_j^{\mathrm{H}}\widehat{\boldsymbol{h}}_1 + \sigma^2\widehat{\boldsymbol{h}}_1^{\mathrm{H}}\widehat{\boldsymbol{h}}_1}. \tag{6}$$

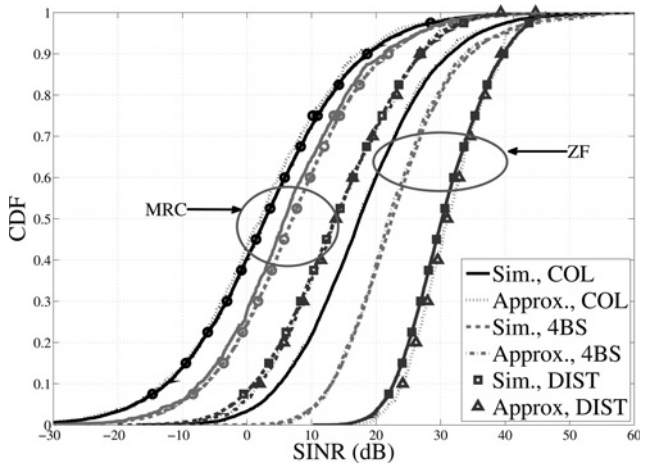

Fig. 3 *SINR CDFs for the three deployment scenarios with ZF and MRC and $r_0 = 1$. nCells = 19, reuse 3*

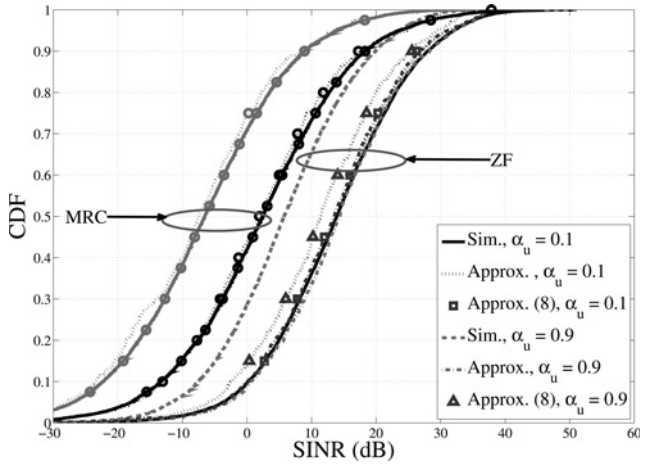

Fig. 4 *SINR CDFs for the COL scenario with ZF and MRC for $r_0 = 0.99$ and different correlation levels, $\alpha_u = \{0.1, 0.9\}$. nCells = 19, reuse 3*

decomposition of $\boldsymbol{R}_r$ gives

$$\breve{\boldsymbol{x}}^H \breve{\boldsymbol{y}} = \tilde{\boldsymbol{x}}^H \boldsymbol{\Psi}^H \boldsymbol{\Lambda} \boldsymbol{\Psi} \tilde{\boldsymbol{y}}, \tag{7}$$

where $\boldsymbol{\Psi} = \text{diag}(\boldsymbol{\Psi}_b, \ldots, \boldsymbol{\Psi}_b)$ and $\boldsymbol{\Lambda} = \text{diag}(\boldsymbol{\Lambda}_b, \ldots, \boldsymbol{\Lambda}_b)$. Furthermore, since $\boldsymbol{\Psi}$ is block diagonal and each UE has the same power in each block, $\boldsymbol{\Psi}\tilde{\boldsymbol{x}}$ is statistically identical to $\tilde{\boldsymbol{x}}$. Hence, $\breve{\boldsymbol{x}}^H \breve{\boldsymbol{y}}$ is statistically identical to $\tilde{\boldsymbol{x}}^H \boldsymbol{\Lambda} \tilde{\boldsymbol{y}} = \tilde{\boldsymbol{x}}^H \boldsymbol{\Lambda}^{1/2} \boldsymbol{\Lambda}^{1/2} \tilde{\boldsymbol{y}}$. Now $\boldsymbol{\Lambda}^{1/2}\tilde{\boldsymbol{y}}$ and $\tilde{\boldsymbol{x}}^H \boldsymbol{\Lambda}^{1/2}$ are simply scaled versions of the original $\tilde{\boldsymbol{x}}, \tilde{\boldsymbol{y}}$ values. Hence, for our uplink model of distributed single-antenna transmitters, the effect of correlation is equivalent to scaling the power at antenna i by Λ_{ii}. As a result, in the subsequent analysis, we replace P_{ij} by $\bar{P}_{ij} = \Lambda_{ii} P_{ij}$ and Q_{ij} by $\bar{Q}_{ij} = \Lambda_{ii} Q_{ij}$ and maintain the independence of the channel correlation coefficients as the correlation is catered for by the power scaling. Note that in the uncorrelated case, $\boldsymbol{R}_r = \boldsymbol{\Lambda} = \boldsymbol{I}$ and the power scaling has no effect, as desired.

4.2 SINR approximation analysis with ZF

Using the full SINR representation in (5) leads to a complicated analysis without any resulting insight. To avoid this complexity, we can approximate the interference from outside the desired cell as noise and replace the estimation error, interference and noise covariance matrix, $(1 - r_0^2)\boldsymbol{E}\boldsymbol{E}^H + \boldsymbol{F}\boldsymbol{F}^H + \sigma^2 \boldsymbol{I}$, by an equivalent noise covariance matrix, $\sigma_{eq}^2 \boldsymbol{I}$, where $\sigma_{eq}^2 = \sigma^2 + 1/N_r (1 - r_0^2) \sum_{i=1}^{N_r} \sum_{j=1}^{N_t} \bar{P}_{ij} + 1/N_r \sum_{i=1}^{N_r} \sum_{j=1}^{N_f} \bar{Q}_{ij}$. The accuracy of this approximation investigated in Section 5 (see Figs. 3 and 4). Thus,

$$\text{SINR}_1^{(ZF)} \simeq \frac{r_0^2}{\sigma_{eq}^2 \left[\left(\widehat{\boldsymbol{H}}^H \widehat{\boldsymbol{H}} \right)^{-1} \right]_{11}}. \tag{8}$$

Using the co-factor expression for $\left[\left(\widehat{\boldsymbol{H}}^H \widehat{\boldsymbol{H}} \right)^{-1} \right]_{11}$, we obtain

$$\frac{r_0^2}{\sigma_{eq}^2 \left[\left(\widehat{\boldsymbol{H}}^H \widehat{\boldsymbol{H}} \right)^{-1} \right]_{11}} = \frac{r_0^2 \left| \widehat{\boldsymbol{H}}^H \widehat{\boldsymbol{H}} \right|}{\sigma_{eq}^2 \left| \widehat{\boldsymbol{H}}_2^H \widehat{\boldsymbol{H}}_2 \right|}, \tag{9}$$

where $\widehat{\boldsymbol{H}}_2$ is the channel matrix, $\widehat{\boldsymbol{H}}$, with the first column removed. The mean SINR over the fast fading can be approximated using the Laplace approximation approach from [21], which was shown to be quite accurate for ratios of quadratic forms in [22], as

$$E\left[\text{SINR}_1^{(ZF)} \right] \simeq \frac{r_0^2 E\left[\left| \widehat{\boldsymbol{H}}^H \widehat{\boldsymbol{H}} \right| \right]}{\sigma_{eq}^2 E\left[\left| \widehat{\boldsymbol{H}}_2^H \widehat{\boldsymbol{H}}_2 \right| \right]} = \frac{r_0^2 \text{Perm}(\bar{\boldsymbol{P}})}{\sigma_{eq}^2 \text{Perm}(\bar{\boldsymbol{P}}_2)}, \tag{10}$$

where Perm(.) is the permanent of a matrix, $\bar{\boldsymbol{P}} = \left(\bar{P}_{ij} \right)$, $1 \le i \le N_r$, $1 \le j \le N_t$, $\bar{\boldsymbol{P}}_2 = \left(\bar{P}_{ij} \right)$, $1 \le i \le N_r$, $2 \le j \le N_t$ and the expectations are with respect to the fast fading. There are several reasons for using the Laplace approximation. The results, shown in Figs. 3 and 4, verify its accuracy for this situation and the analytical results in (13)–(17) verify the simple form of the resulting expressions. Furthermore, [21, 22] suggest that an exact analysis is intractable for more than two UEs. Rewriting the right-hand side of (10) gives:

$$\begin{aligned} \frac{r_0^2 \text{Perm}(\bar{\boldsymbol{P}})}{\sigma_{eq}^2 \text{Perm}(\bar{\boldsymbol{P}}_2)} &\simeq \frac{r_0^2 \sum_{i_1=1}^{N_r} \bar{P}_{i_1 1} \sum_{i_2 \in s(1,1)} \bar{P}_{i_2 2} \cdots \sum_{i_{N_t} \in s(1,N_t-1)} \bar{P}_{i_{N_t} N_t}}{\sigma_{eq}^2 \sum_{i_2=1}^{N_r} \bar{P}_{i_2 2} \cdots \sum_{i_{N_t} \in s(2,N_t-1)} \bar{P}_{i_{N_t} N_t}} \\ &= \frac{r_0^2 \sum_{i_1=1}^{N_r} \bar{P}_{i_1 1} \left[\bar{G} - \sum_{j=2}^{N_t} F_j(i_1) \right]}{\sigma_{eq}^2 \bar{G}} \\ &= \frac{r_0^2 \sum_{i_1=1}^{N_r} \bar{P}_{i_1 1}}{\sigma_{eq}^2} - \frac{r_0^2 \sum_{i_1=1}^{N_r} \bar{P}_{i_1 1} \sum_{j=2}^{N_t} F_j(i_1)}{\sigma_{eq}^2 \bar{G}}, \end{aligned} \tag{11}$$

where $s(k, l) = \{1, 2, \ldots N_r\} \backslash \{i_k, i_{k+1}, \ldots, i_l\}$, $\bar{G} = \sum_{i_2=1}^{N_r} \bar{P}_{i_2 2} \cdots \sum_{i_{N_t} \in s(2,N_t-1)} \bar{P}_{i_{N_t} N_t}$ and $F_j(i_1)$ is defined as (see (12))

For $N_r \gg N_t$, the number of products of powers in $\bar{G}$ dominates the number in $\sum_{j=2}^{N_t} F_j(i_1)$ and therefore $\bar{G} \gg \sum_{j=2}^{N_t} F_j(i_1)$ so that

$$E\left[\text{SINR}_1^{(ZF)} \right] \simeq r_0^2 \sum_{i=1}^{N_r} \bar{P}_{i1} \Big/ \sigma_{eq}^2. \tag{13}$$

Note that (13) relies on the equivalent noise model (see (8)), the Laplace approximation (see (10)) and the removal of lower order terms in (11). The latter two approximations are motivated by massive MIMO properties while the first is required for analytical

$$F_j(i_1) = \bar{P}_{i_1 j} \sum_{i_2 \in s(1,1)} \bar{P}_{i_2 2} \cdots \sum_{i_{j-1} \in s(1,j-2)} \bar{P}_{i_{j-1} j-1} \sum_{i_{j+1} \in s(1,j)} \bar{P}_{i_{j+1} j+1} \cdots \sum_{i_{N_t} \in s(1,N_t-1)} \bar{P}_{i_{N_t} N_t}. \tag{12}$$

progress. The overall accuracy and the accuracy of the Laplace approximation stage are evaluated in Section 5.

4.3 SINR approximation analysis with MRC

The mean SINR is again approximated using a Laplace approximation (as in (10)) to give (see (14))

Similar results were obtained in [5] from a different approach, but were not expressed or used in the same way as in the following. In the massive MIMO scenario, the system is intra-cell interference limited and the leading term in both the numerator and denominator of (14) is dominant. As a result,

$$E\left[\mathrm{SINR}_1^{(\mathrm{MRC})}\right] \simeq \frac{r_0^2 \sum_{i=1}^{N_\mathrm{r}} \bar{P}_{i1}}{\left[\sum_{i=1}^{N_\mathrm{r}} \bar{P}_{i1}\left(-r_0^2 \bar{P}_{i1} + \sum_{j=1}^{N_\mathrm{t}} \bar{P}_{ij}\right)\right] / \left[\sum_{k=1}^{N_\mathrm{r}} \bar{P}_{k1}\right]}. \tag{15}$$

4.4 Discussion

The simple approximations in (13) and (15) provide the following insights. Increasing the transmit SNR, ρ, does not scale (13) linearly as ZF only removes the intra-cell interference resulting in a ceiling on the ZF SINR. In addition, for MRC, (15) is independent of ρ as MRC is interference limited and a higher transmit SNR does not help. Consider the case of perfect CSI, $r_0 = 1$, for further insights. To evaluate the effects of distributed antennas, we substitute $\bar{P}_{ij} = \bar{P}_j$ into (13) and (15) to obtain the co-located results:

$$E\left[\mathrm{SINR}_1^{(\mathrm{ZF})}\right] \simeq \frac{N_\mathrm{r} \bar{P}_1}{\sigma_{\mathrm{eq}}^2}, \quad E\left[\mathrm{SINR}_1^{(\mathrm{MRC})}\right] \simeq N_\mathrm{r} \frac{\bar{P}_1}{\sum_{t=2}^{N_\mathrm{t}} \bar{P}_\mathrm{t}}. \tag{16}$$

In the BBS scenario, using $\bar{P}_{ij} = \bar{P}_j^{(k)}$, where $k \in \{1, \ldots, B\}$, (13) and (15) simplify to

$$E\left[\mathrm{SINR}_1^{(\mathrm{ZF})}\right] \simeq \frac{N_\mathrm{r}}{B} \frac{\sum_{k=1}^{B} \bar{P}_1^{(k)}}{\sigma_{\mathrm{eq}}^2},$$

$$E\left[\mathrm{SINR}_1^{(\mathrm{MRC})}\right] \simeq \frac{N_\mathrm{r}}{B} \frac{\sum_{k=1}^{B} \bar{P}_1^{(k)}}{\sum_{k=1}^{B} \left(\left[\bar{P}_1^{(k)}\right] / \left[\sum_{i=1}^{B} \bar{P}_1^{(i)}\right]\right) \sum_{r=2}^{N_\mathrm{t}} \bar{P}_\mathrm{r}^{(k)}}. \tag{17}$$

Note that the results in (13)–(17) are averaged over the fast fading. Nevertheless, we use these results as approximations to the instantaneous SINR at a system level as the variation due to the fast fading is negligible compared with the variation due to the long term powers. As an example, the coefficient of variation (CV) of the square of the absolute fast fading term, $|U_{ij}|^2$, is $CV = 1$ whereas for $\sigma_{\mathrm{SF}} = 8$ dB, $\gamma = 3$ the CV of $\bar{P}_{ij}$, exceeds 50 (where the CV is computed using the moments derived in [23] for a circular cell). This difference is massive on the CV scale. The validity of the approximations is also supported by the accuracy of the results in Fig. 3.

The MRC result in (16) is similar to the SINR of a large code division multiple access system [24, (8)]; however, the assumptions and channels are significantly different. The ZF result also differ from previously published results [5, 24]. Comparing (13) with (16) and (17) for $r_0 = 1$, we observe that the form of the ZF SINR is the same, but the co-located version has a single power, $\bar{P}_1$, scaled by $N_\mathrm{r}/\sigma_{\mathrm{eq}}^2$; the BBS version has the average of

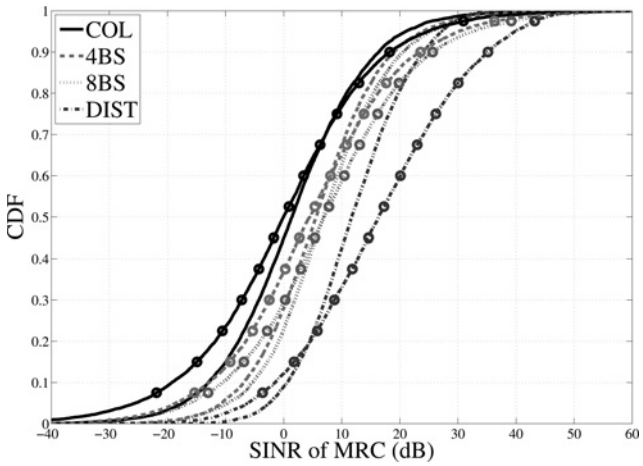

Fig. 5 *SINR CDFs for the four deployment scenarios with ZF, $\gamma \in \{3, 4\}$. Lines alone represent $\gamma = 3$ and lines with markers represent $\gamma = 4$. nCells = 19*

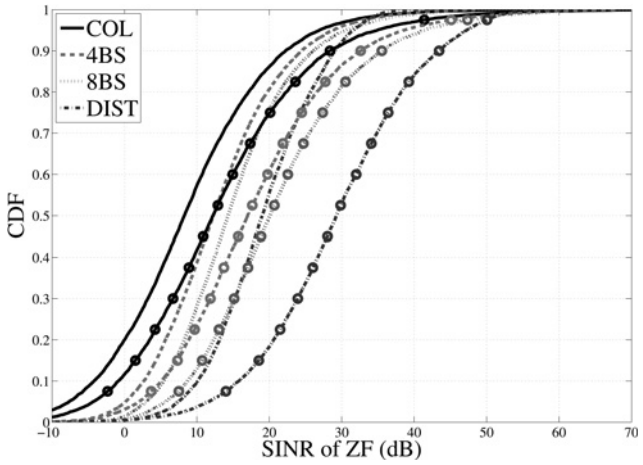

Fig. 6 *SINR CDFs for the four deployment scenarios with MRC, $\gamma \in \{3, 4\}$. Lines alone represent $\gamma = 3$ and lines with markers represent $\gamma = 4$. nCells = 19*

B powers $\sum_{k=1}^{B} \bar{P}_1^{(k)}/B$ scaled by $N_\mathrm{r}/\left(\sigma_{\mathrm{eq}}^2\right)$ and the distributed version has the average of N_r different powers, $\bar{P}_{i1}$, scaled by $N_\mathrm{r}/\sigma_{\mathrm{eq}}^2$. Hence, the mean of the absolute SINR is very similar for the three cases, but in the BBS and the distributed case the variation is heavily reduced due to increased averaging. Thus, the co-located case has higher maximum values (all N_r links are strong when the UE is in a good location) but suffers from a poor lower tail (when all N_r links are weak). The lower tail of the cumulative distribution function (CDF) is critical and is emphasised with a dB scale showing that the distributed case will outperform the co-located case considerably (see Figs. 3, 5, 6). The BBS scenario is important because it is much easier to locate a few BSs around the cell rather than use DIST. Hence, this scenario enables us to investigate how much of the fully distributed gains are achieved from a layout with only B sites. The same conclusions can be drawn for MRC, since the ratio of two single variables in (16) is being compared with the ratio of an average to a weighted average in (15) and (17). Again, with a distributed array, the averaging

$$E\left[\mathrm{SINR}_1^{(\mathrm{MRC})}\right] \simeq \frac{r_0^2\left(\sum_{i=1}^{N_\mathrm{r}} \bar{P}_{i1}\right)^2 + r_0^2 \sum_{i=1}^{N_\mathrm{r}} \bar{P}_{i1}^2}{r_0^2 \sum_{i=1}^{N_\mathrm{r}} \sum_{j=2}^{N_\mathrm{t}} \bar{P}_{i1}\bar{P}_{ij} + \left(1 - r_0^2\right) \sum_{i=1}^{N_\mathrm{r}} \sum_{j=1}^{N_\mathrm{t}} \bar{P}_{i1}\bar{P}_{ij} + \sum_{i=1}^{N_\mathrm{r}} \sum_{j=1}^{N_\mathrm{f}} \bar{P}_{i1}\bar{Q}_{ij} + \sigma^2 \sum_{i=1}^{N_\mathrm{r}} \bar{P}_{i1}}. \tag{14}$$

will reduce the variation leading to considerable improvement in the lower tail. Note that the averaging due to distributed antennas has a greater impact when the equivalent link gains are more variable, that is, when the path loss exponent is higher or when the shadow fading correlation is smaller. The improvements of distributed arrays have been explained via (13) and (15)–(17) in terms of an averaging effect. This is closely linked to the benefits of reduced link distances with distributed arrays. Spreading the antennas creates a range of link distances and most UEs will be in close proximity to some antennas and distant from others. As a result, extreme cases with all short or long links are removed and most UEs have a few short links. Therefore, these antenna proximity benefits can be viewed as an averaging effect.

5 SINR results using analysis and simulation

In this section, we verify the accuracy of the analysis in Section 4 and investigate the effects of system size, deployment and propagation parameters via Monte Carlo simulation. The baseline parameters are: $N_r = 128$, $N_t = 10$, $\rho = 0$ dB, $\gamma = 3$, $\sigma_{SF} = 8$ dB. Each cell is assumed to have a radius of $r = 0.5$ units, $b = 1/5$, $d_a = 0$ for COL, $d_a = 0.7$ for 4BS, $d_a = 0.6$ for 8BS, and $d_a = 1$ for DIST. The value of d_a selected for 4BS and 8BS is chosen as it is nearly optimal for both ZF and MRC in the perfect CSI and zero correlation condition. For 4BS, the results in Fig. 7 support our choice and for 8BS, similar simulations (not presented here) were used to select d_a. Where these parameters are changed, it is denoted in figure labels or captions. The link distance is calculated with an exclusion zone, so that $d_{ij} > 0.01$, and the scaling parameter, A, in (4) is set to 1. Note that the value of A has a very small impact on the results as in the interference limited cases considered, A is present in the numerator and denominator of the SINR and is essentially cancelled out. This value is fixed across all simulations so we are essentially considering a fixed transmit power. Most of the results correspond to the ideal situation where perfect CSI is available with zero latency and zero correlation. These assumptions are much harder to emulate for distributed arrays. Furthermore, the simulated instantaneous SINR values include fast fading. With this background, the numerical results in Figs. 2–7 are discussed below.

Fig. 2 shows the SINR for DIST with MRC and ZF and differing levels of interference. For MRC, intra-cell interference is not nulled and is dominant. Hence, all four interference scenarios have similar SINR distributions. For ZF, intra-cell interference is nulled and so the interference scenarios have a large effect. Results for nCells $\in \{7, 19\}$ are similar as the tier 1 interferers are dominant. The effect of reuse is large and the (nCells = 19, reuse 3) CDF is shifted up by around 10 dB. Finally, the nCells = 1 result is interference free due to ZF leading to much higher SNRs. Note that similar conclusions are found with COL, 4BS and 8BS deployments.

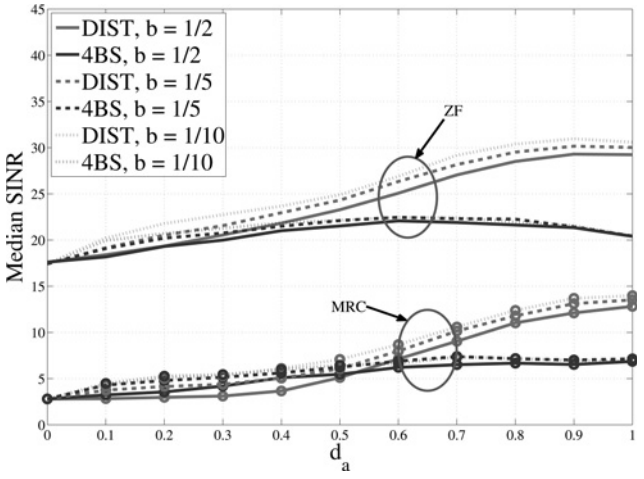

Fig. 7 *Median SINR vs d_a for ZF and MRC with DIST and 4BS with $b \in \{1/2, 1/5, 1/10\}$. Lines alone represent ZF and lines with markers represent MRC. nCells = 19, reuse 3*

Fig. 3 compares the SINR approximations (labelled Approx.) using (13), (8) and (15) with the simulated instantaneous SINR values (labelled Sim.) for MRC and ZF. The remarkably simple approximations in (13) and (15) provide an excellent match to the SINR CDFs for both receivers. This validates the use of the approximation techniques in Section 4. The results in Fig. 3 are for perfect CSI ($r_0 = 1$). When imperfect CSI is considered the analytical results are slightly less accurate as shown in Table 1. For $r_0 \in \{0.6, 1\}$, approximate results for the median SINR are accurate to within 1 dB for all MRC scenarios. For ZF, results are within 1 dB for COL, but have errors around 2 dB for 4BS and DIST. Two other features are shown in Table 1. First, the approximation error increases as r_0 reduces since greater channel estimation error inflates the $\boldsymbol{E}$ matrix making the equivalent noise model less accurate. Secondly, when the CSI is poor 4BS can outperform DIST. This is because DIST often results in a UE having a single dominant link and this situation is particularly susceptible to poor CSI.

For the COL scenario, Fig. 4 compares the SINR approximations, (13), (8) and (15), with simulated instantaneous SINR values for MRC and ZF with imperfect CSI and correlation, $r_0 = 0.99$ and $\alpha_u = \{0.1, 0.9\}$. These results demonstrate that the SINR obtained from the simple approximations in (13) and (15) are less accurate for ZF when the correlation is high, but work well with low correlation. In addition, with low correlation the approximations in (8) are similar to (13) supporting the use of the Laplace approximation. However, for high correlation the ZF approximation is poor. This is caused by the effect of the correlation which makes the aggregate interference and noise more coloured and less like simple additive noise. Overall, the simple closed form approximations are useful for all MRC scenarios and for ZF with low correlation.

Compared with the results in Fig. 3, imperfect CSI has a much greater impact on ZF than MRC. In the DIST scenario, the correlation does not have an impact on the system performance because the correlation matrix $\boldsymbol{R}_r$ is the identity matrix.

Using a frequency reuse of factor 1 (nCells = 19), Figs. 5 and 6 show the effect of γ on ZF and MRC. As shown analytically in Section 4, increasing γ increases the gap between the co-located and distributed results. The changes between $\gamma = 3$ and $\gamma = 4$ are more notable for ZF than for MRC since an increased γ has a direct effect on SINR for ZF, whereas for MRC, increasing γ affects both the numerator and denominator of (15). Changes are also more notable for the distributed scenario. Increased path loss accentuates the variability in link gain. This is ideal for DIST where the different antenna locations mean that different UEs tend to find different sets of antennas with reasonable link gains and the greater path loss from other UEs reduces the overall interference which must be mitigated. Importantly, Figs. 5 and 6

Table 1 Simulated and approximated median SINR (dB) with imperfect channel estimation

r_0	Sim.			Approx.		
	COL	4BS	DIST	COL	4BS	DIST
ZF (nCells = 19, reuse 3)						
1	17.2	22.2	30.1	17.3	22.2	30.8
0.99	14.1	18.5	20.0	14.1	17.7	22.4
0.9	7.7	11.6	10.3	7.5	10.0	12.6
0.8	4.6	8.1	6.7	4.2	6.3	8.8
0.6	−0.1	3.3	1.6	−0.5	1.6	3.9
MRC (nCells = 19, reuse 3)						
1	3.0	6.9	13.0	2.4	6.2	12.9
0.99	2.9	6.8	11.6	2.1	6.1	12.2
0.9	2.1	5.9	7.0	1.4	5.2	6.9
0.8	0.9	4.8	4.5	0.2	4.0	3.7
0.6	−1.5	2.2	0.4	−2.4	1.4	−0.5

Table 2 Median SINR (dB) with imperfect channel estimation and correlation

r_0	ZF				MRC			
	COL	4BS	8BS	DIST	COL	4BS	8BS	DIST
$\alpha_u = 0.1$ (*n*Cells = 19, reuse 3)								
1	17.5	22	24	30	3.0	7.1	8.3	13
0.99	14	18.5	20.1	20.2	2.8	6.9	7.9	12
0.9	7.6	11.5	12.3	10	1.9	5.8	7.2	7.0
0.8	4.7	7.9	8.9	6.6	1.4	4.9	5.8	4.4
0.6	0.1	3.4	3.9	1.7	−1.3	2.9	2.8	0.4
$\alpha_u = 0.9$ (*n*Cells = 19, reuse 3)								
1	8.9	14	17	30	−6.4	−1.7	0.3	13
0.99	5.8	10	13	20	−6.7	−2.1	0.01	12
0.9	−0.5	3.5	5.5	10	−7.4	−3.2	−0.7	7.0
0.8	−3.6	0.3	1.9	6.6	−8.2	−3.9	−2.2	4.5
0.6	−8.1	−4.5	−3	1.7	−11	−6.5	−5.2	0.4

quantify the gains offered by 4BS and 8BS in comparison with DIST. A fully distributed array may be impractical and only a partial distribution, an intermediate deployment as in 4BS or 8BS, may be viable. We observe that for ZF, moving from one BS site to four provides approximately 38% of the gains in moving from one site to 128 sites. The corresponding percentage gain is approximately 40% for MRC. Moving from one BS site to eight provides approximately 56% of the gains in moving from one site to 128 sites for ZF. The corresponding percentage gain is approximately 53% for MRC. With reuse 3, the percentage gains are similar.

Fig. 7 shows the median SINR of ZF and MRC with different values of d_a and b for DIST and 4BS. This explores the effect of spreading the antennas over increasing proportions of the cell area (increasing d_a) and the effect of increasing shadow fading correlation (increasing b). We observe that increasing the spread of the antenna array is more beneficial for DIST compared with 4BS and for ZF compared with MRC. The effects of shadow fading correlation is less pronounced but in all cases, increasing correlation reduces SINR. Both effects are due to the averaging effect explained by the closed form analysis in Section 4.

Obtaining accurate CSI is one of the challenges in massive MIMO as performance can be limited by interference arising from the re-use of pilots in neighbouring cells [2]. Correlation is also an important factor when large numbers of antennas are deployed in a small physical volume. In Table 2, we give median SINR results for the four scenarios and both linear receivers for varying levels of CSI and correlation. Clearly, ZF is more sensitive to imperfect CSI in all deployments and the gains of ZF over MRC are reduced as r_0 decreases, particularly for DIST. DIST is more heavily affected by imperfect CSI than COL. With imperfect CSI, the additive channel errors in the desired channel are of the form $\sqrt{1-r_0^2}\boldsymbol{e}_m$, where $\boldsymbol{e}_m$ is the mth column of $\boldsymbol{E}$. The power of this term is $\left(1-r_0^2\right)\sum_{i=1}^{N_r}\bar{P}_{im}$ and as shown in Section 4, this is larger for DIST than COL. Hence, imperfect CSI has a greater impact on DIST than on COL as mentioned in the discussion of Table 1. Both r_0 and α_u have a serious impact on performance, although DIST is unaffected by correlation as there are no co-located antennas. Again, we observe that imperfect CSI can cause 4BS or 8BS to outperform DIST.

To summarize the practical implications of the numerical results, some level of distribution is preferable as averaging reduces variation and correlation has less impact on performance. Since urban channels tend to have higher σ_{SF} and γ values than most environments, they are usually more variable and therefore will benefit more from the averaging effects of distributed arrays. However, it is far easier to locate a few BSs around a cell than to use the full DIST approach. Hence, there is a performance-complexity trade-off which is also influenced by the fact that distributed arrays are likely to have less accurate CSI than co-located arrays. As a result, an intermediate deployment is an appealing design choice as it is simpler and less sensitive to CSI quality than DIST while avoiding the spatial correlation problems of COL.

6 Conclusion

We investigated the interactions between deployment scenarios, ZF, MRC and propagation parameters. A mixture of analysis, simulation and physical interpretations were used to show that the improvements offered by distributed arrays are largely due to an averaging effect which is more prominent for the ZF case. This averaging improves the lower tail of the SINR CDF of the distributed case relative to the co-located case. We also show that imperfect CSI has a significant impact which is greater for distributed arrays than for co-located arrays and reduces the improvements offered by ZF. In addition, correlation does not play a role in degrading the performance in distributed arrays but strongly affects co-located deployments. As a result, a partially distributed ZF system is an ideal candidate if the cost and CSI requirements could be met, providing performance benefits and robustness to errors in CSI.

7 References

1 Hoydis, J., Brink, S.T., Debbah, M.: 'Massive MIMO in the UL/DL of cellular networks: how many antennas do we need?', *IEEE J. Sel. Areas Commun.*, 2013, **31**, (2), pp. 160–171
2 Rusek, F., Persson, D., Lau, B.K., *et al.*: 'Scaling up MIMO: Opportunities and challenges with very large arrays', *IEEE Signal Process. Mag.*, 2013, **30**, (1), pp. 40–60
3 Ngo, H.Q., Larsson, E.G., Marzetta, T.L.: 'Uplink power efficiency of multiuser MIMO with very large antenna arrays'. Proc. IEEE Conf. Allerton, Monticello, IL, September 2011, pp. 1272–1279
4 Hoydis, J., Debbah, M.: 'Green networks: Small cells or massive MIMO?'. Methodological Foundations on Green Radio, Telecom Paristech, France, 2012
5 Truong, K.T., Heath, R.W.: 'The viability of distributed antennas for massive MIMO systems'. Proc. 2013 IEEE Conf. Asilomar, Pacific Grove, CA, November 2013, pp. 1318–1323
6 Liu, Z., Dai, L.: 'A comparative study of downlink MIMO cellular networks with co-located and distributed base-station antennas', *IEEE Trans. Wirel. Commun.*, 2014, **13**, (11), pp. 6259–6274
7 Liu, A., Lau, V.K.N.: 'Joint power and antenna selection optimization for energy-efficient large distributed MIMO networks'. Proc. IEEE Conf. ICCS, Singapore, November 2012, pp. 230–234
8 Dai, H.: 'Distributed versus co-located MIMO systems with correlated fading and shadowing'. Proc. IEEE Conf. ICASSP, Toulouse, May 2006, 4, pp. 561–564
9 Clark, M.V., III Willis, T., III Greenstein, L.J., *et al.*: 'Distributed versus centralized antenna arrays in broadband wireless networks'. Proc. 2001 IEEE Conf. VTC, Rhodes, May 2001, pp. 33–37
10 Schwarz, S., Heath, R.W. Jr., Rupp, M.: 'Single-user MIMO versus multi-user MIMO in distributed antenna systems with limited feedback', *Springer EURASIP J. Adv. Signal Process.*, 2013, **1**, pp. 1–20
11 Irmer, R., Droste, H., Marsch, P., *et al.*: 'Coordinated multipoint: concepts, performance, and field trial results', *IEEE Commun. Mag.*, 2011, **49**, (2), pp. 102–111
12 Rezki, Z., Alouini, M.: 'Ergodic capacity of cognitive radio under imperfect channel-state information', *IEEE Trans. Veh. Technol.*, 2012, **61**, (5), pp. 2108–2119
13 Hoydis, J., Kobayashi, M., Debbah, M.: 'Asymptotic performance of linear receivers in network MIMO'. Proc. IEEE Conf. ASILOMAR, Pacific Grove, CA, November 2010, pp. 942–948
14 Bai, L., Choi, J.: 'Low complexity MIMO detection' (Springer Science & Business Media, New York, 2012)
15 Stuber, G.L.: 'Principles of mobile communication' (Springer Science & Business Media, New York, 2011)
16 Rappaport, T.S.: 'Wireless communications: principles and practice' (Prentice Hall PTR, New Jersey, 1996)
17 Gudmundson, M.: 'Correlation model for shadow fading in mobile radio systems', *Electron. Lett.*, 1991, **27**, (23), pp. 2145–2146
18 Weitzen, J., Lowe, T.J.: 'Measurement of angular and distance correlation properties of log-normal shadowing at 1900MHz and its application to design of PCS systems', *IEEE Trans. Veh. Technol.*, 2002, **51**, (2), pp. 265–273
19 Loyka, S.L.: 'Channel capacity of MIMO architecture using the exponential correlation matrix', *IEEE Commun. Lett.*, 2001, **5**, (9), pp. 369–371
20 Kopsa, K., Matz, G., Artés, H., Hlawatsch, F.: 'Bit error rate estimation for a joint detection receiver in the downlink of UMTS/TDD'. Proc. IEEE Conf. IST Mobile and Wireless Communications, Aveiro, Portugal, June 2009, pp. 256–260
21 Basnayaka, D.A., Smith, P.J., Martin, P.A.: 'Performance analysis of macrodiversity MIMO systems with MMSE and ZF receivers in flat Rayleigh fading', *IEEE Trans. Wirel. Commun.*, 2013, **12**, (5), pp. 2240–2251
22 Lieberman, O.: 'A Laplace approximation to the moments of a ratio of quadratic forms', *Biometrika*, 1994, **81**, (4), pp. 681–690
23 Hanif, M.F., Shafi, M., Smith, P.J., Dmochowski, P.: 'Interference and deployment issues for cognitive radio systems in shadowing environments'. Proc. IEEE Conf. ICC, Dresden, June 2009, pp. 1–6
24 Tse, D.N.C., Hanly, S.V.: 'Linear multiuser receivers: effective interference, effective bandwidth and user capacity', *IEEE Trans. Inf. Theory*, 1999, **45**, (2), pp. 641–657